Available online at www.sciencedirect.com
ScienceDirect
Trans. Nonferrous Met. Soc. China 27(2017) 1785−1793
Transactions of Nonferrous Metals Society of China
www.tnmsc.cn

Synthesis of $NiMoO_4$ nanoparticles by sol−gel method and their structural, morphological, optical, magnetic and photocatlytic properties

V. UMAPATHY[1,2], P. NEERAJA[3], A. MANIKANDAN[4], P. RAMU[5]

1. Research and Development Centre, Bharathiar University, Coimbatore, Tamil Nadu 641046, India;
2. Caplin Point Laboratories Limited, Chennai 600017, India;
3. Department of Chemistry, NKR Government Arts College for Women, Namakkal, Tamil Nadu 637001, India;
4. Department of Chemistry, Bharath Institute of Higher Education and Research, Bharath University, Chennai 600073, India;
5. Department of Chemistry, Meenakshi Academy of Higher Education and Research, Chennai, Tamil Nadu 600078, India

Received 9 June 2016; accepted 20 March 2017

Abstract: Nickel molybdate ($NiMoO_4$) nanoparticles (NPs) were synthesized by sol−gel method. Utilizing water as solvent provides crystalline nanostructures. These nanocrystals were structurally characterized by X-ray diffraction, energy dispersive X-ray analysis (EDX), and Fourier transform infrared spectra. Compositional stoichiometry was confirmed by EDX technique. The size and shape were observed by scanning electron microscopy (SEM) and transmission electron microscope (TEM). It was found that the obtained NPs were pure and single phase crystalline with monoclinic structure. The optical properties were studied by ultraviolet−visible diffuse reflectance spectroscopy (UV−Vis−DRS) and photoluminescence (PL) measurements at room temperature. The magnetic properties were studied by vibrating sample magnetometer (VSM) and results showed superparamagnetic behavior of the obtained nanoparticles. Photocatalytic activity of $NiMoO_4$ was studied. The photocatalytic activity of $NiMoO_4$ was enhanced with the addition of TiO_2. The catalysts $NiMoO_4$, TiO_2 and $NiMoO_4$−TiO_2 nanocomposites (NC) were tested for photocatalytic degradation (PCD) of 4-chlorophenol (4-CP). It was found that PCD efficiency of $NiMoO_4$−TiO_2 NC was higher than that of pure $NiMoO_4$ and TiO_2.
Key words: $NiMoO_4$; TiO_2; nanostructure; sol−gel synthesis; optical properties; magnetic properties; photo-catalysis; monoclinic structure

1 Introduction

Nano-structured semiconductor materials have attracted considerable attention in nanoscience and nanotechnology due to their better physico-chemical properties compared with their same bulk materials [1]. Recently, metal molybdate materials have been widely used in photoluminescence, microwave applications, optical fibers, scintillator materials, humidity sensors and photo-catalysis [2,3]. Nickel molybadate ($NiMoO_4$) possesses various applications in catalysts such as oxidative dehydrogenation of light alkanes [4,5], hydrodesulfurization and hydrodenitrogenation [6,7]. Several methods have been used to synthesize this metal oxide such as sonochemical, hydrothermal, sol−gel, chemical precipitation methods [8−17]. Among many metal molybdates, $NiMoO_4$ is one of the important photocatalyst for degradation of organic compounds.

Various methods have been used to prepare $NiMoO_4$ nanostrutures such as co-precipitation [18,19], microwave-assisted solvothermal [20], mechano-chemical [21], sonochemical [22], microwave sintering [23], and hydrothermal [24] methods. However, by using the above conventional methods, $NiMoO_4$ nanoparticles were produced comparatively large in size with irregular morphology and inhomogeneity. In the present study, ethyl cellulose was used as surfactant to prepare $NiMoO_4$ nanoparticles by sol−gel method. This surfactant is a derivative of cellulose, some of hydroxyl groups on the repeating glucose units are converted into ethyl ether groups. This hydroxyl group plays an important role in the dispersion process of $NiMoO_4$ particles. During reaction, ester linkage forms between hydroxyl group in

Corresponding author: P. NEERAJA; Tel: +91-9487819133; E-mail: researchneeraja@gmail.com
DOI: 10.1016/S1003-6326(17)60201-2

ethyl cellulose and carboxylic group in citric acid. The ester linkage forms large polymeric structure which traps the metal oxides and water molecules, and thus prevents the agglomeration of particles [25,26]. Sol−gel method exhibits many advantages over other methods, such as simplicity, low process temperature and high control of pure products.

Nanosized photocatalytic materials have gained much importance due to their prospective uses in the control of environmental pollution [26,27], conversion of solar energy [28] and production of hydrogen by spilling of water [25]. Photocatalysis offers good-quality technology for the removal of different toxic organic compounds from water by using TiO_2 as catalyst has been studied [29], because of economic and ecologically safe opportunity for solving energy and pollution problems [30]. Many nanostructured mixed oxides, such as tantalates [31,32], vanadates [33,34], molybdates [35−37] and tungstates [26,27,38−41], have been reported for UV and visible−light photocatalytic activities.

There are several studies on the synthesis of metal molybdates by sol−gel method, characterization and photocatalytic activities. UMAPATHY et al [35,36] carried out synthesis by sol−gel method, characterization and photocatalytic activity of bismuth molybdate [35] and ferric molybdate [36]. UMAPATHY and NEERAJA [37] reported on sol−gel synthesis, characterization and photocatalytic activity of cobalt molybdate.

$NiMoO_4$ is a good UV−Vis light-driven photocatalytic activity for splitting of water and degradation of organic pollutants [42]. The photocatalytic activity of $NiMoO_4$ can be improved by doping with TiO_2. Such superior $NiMoO_4$−TiO_2 mixed catalyst lengthens its application through the generation of new catalytic sites, due to strong interaction between them. Therefore, it is attractive to study the photocatalytic activity of $NiMoO_4$−TiO_2 mixed oxides. In the present study, $NiMoO_4$ nanoparticles (NPs) were prepared by sol−gel method and it was observed that $NiMoO_4$ NPs can be used as a photocatalyst for the efficient bleaching and mineralization of 4-chloro phenol (4-CP) under UV−Vis light irradiation.

2 Experimental

2.1 Materials and methods

Chemicals used in this study were of analytical grade obtained from Merck, India and were used as received without further purification. Ammonium molybdate ($(NH_4)_6Mo_7O_{24}\cdot 4H_2O$), nickel nitrate ($Ni(NO_3)_2\cdot 6H_2O$), citric acid and ethyl cellulose were used for the sol−gel method. 3 g of ethyl cellulose powder (degree of substitution (DS) of ethyl group ~ 1.2) was sprinkled slowly into warm deionized water at 50 °C under continuous stirring to avoid clumping of the material. 17.7 g of ammonium molybdate was dissolved in 50 mL of deionized water, 29.1 g of nickel nitrate was dissolved in 50 mL deionized water and 10 g of citric acid was dissolved in 50 mL deionized water, separately. These solutions were added to ethyl cellulose solution slowly with constant stirring at 50 °C to form sol. This sol was then heated slowly to 90 °C under constant stirring to obtain a wet gel. Then, the wet gel product was dried over 105 °C for 1 h in hot air oven and then calcined at 650 °C for 2 h. It was ground in a mortar to form a final product of fine powder.

2.2 Characterization

The characterization of the $NiMoO_4$ nano-powders obtained was carried out by using different methods to verify the formation of crystal, size of crystallite, distribution and other parameters. Rigaku Ultima X-ray diffractometer equipped with Cu K_α radiation (λ=1.5418 Å) was used to analyze the structural characterization of $NiMoO_4$ nanoparticles. Perkin Elmer FT-IR spectrometer was used to analyze the surface functional groups. Jeol JSM6360 scanning electron microscopy (SEM) was used to analyze morphologies and energy dispersive X-ray analysis (EDX) and transmission electron microscopy (TEM) analysis were performed with Philips PM 200 transmission electron microscopy. DRS spectra were recorded by using Cary100 UV−Vis spectrophotometer to estimate their band gap energy (E_g). Varian Cary eclipse fluorescence spectrophotometer was used to record photoluminescence (PL_T) spectra. PMC MicroMag 3900 model vibrating sample magnetometer (VSM) equipped with 1 T magnet was used for magnetic measurements at room temperature.

2.3 Photocatalytic reactor setup and degradation procedure

A self-designed photocatalytic reactor was used to perform all photochemical reactions under identical conditions. This reactor consists of eight medium pressure mercury vapor lamps (8 W) set in parallel and emitting 365 nm of light. The reactor has a reaction chamber with specially designed reflectors made of highly polished aluminium and built in cooling fan at the bottom and black cover to prevent leakage of light. Magnetic stirrer was placed at the center of reaction chamber. The open borosilicate glass tube with 40 cm in height and 12.6 mm in diameter was used as a reaction vessel. Only six parallel mercury lamps were used to carry out irradiation. To provide oxygen and for the complete mixing of solution, the solution was aerated continuously by a pump. Prior to photocatalytic analysis, the adsorption of 4-CP on $NiMoO_4$ and TiO_2-supported

$NiMoO_4$ nano photocatalyst was carried out by mixing 100 mL of aqueous solution of 4-CP (50 mg/L) with fixed quantity (0.3 mg/mL) of the respective photocatalyst. A known quantity of commercially available TiO_2 (Degussa P-25) was mixed with a known quantity of $NiMoO_4$ and finely ground in a mortar and pestle for 30 min so as to obtain a uniform mixture of $NiMoO_4$−TiO_2 in the required mole fraction. The PCD was carried out by mixing 100 mL of aqueous 4-CP (50 mg/L) solution with known quantity (0.3 mg/mL) of pure $NiMoO_4$ nano photo-catalyst, pure TiO_2 photo-catalyst and mixed oxides $NiMoO_4$−TiO_2 photo-catalyst, individually. The interactions of $NiMoO_4$ with TiO_2 can be assumed to be those taking place at the grain boundaries. The PCD efficiency was calculated for $NiMoO_4$, TiO_2 and $NiMoO_4$−TiO_2 mixed oxide. All solutions prior to photolysis were kept in dark by covering with aluminium foil to prevent any photochemical reactions. The PCD efficiency (η) was calculated from the following equation:

$$\eta=(C_i-C_t)/C_i\times100\% \quad (1)$$

where C_i is the initial concentration of 4-CP, C_t is the concentration of 4-CP at time t.

3 Results and discussion

3.1 Powder X-ray diffraction (XRD)

The structure of crystal and phase analysis of the sample were characterized by powder X-ray diffraction (XRD). Powder XRD patterns of the as-prepared $NiMoO_4$ NPs shown in Fig. 1 were indexed to monoclinic $NiMoO_4$ according to the JCPDS database No.33-0948 [43−46]. Figure 1 (inset) shows XRD pattern of bulk $NiMoO_4$. Impurities of secondary phases such as NiO, MoO_3, and others were not detected in the XRD pattern. The average crystallite size of $NiMoO_4$ sample was calculated by using Debye−Scherrer formula given in Eq. (2):

$$L=\frac{0.89\lambda}{\beta\cos\theta} \quad (2)$$

where L is the crystallite size, λ is the wavelength of X-ray, θ is the Bragg diffraction angle and β is the full width at half maximum (FWHM). The average crystallite size L calculated from the diffraction peaks was found to be around 19.27 nm. The calculated lattice parameters were found to be a=9.384 Å, b=8.765 Å, and c=8.025 Å, which are in good agreement with the JCPDS file card No. 33-0948.

3.2 FT-IR spectral analysis

Figure 2 shows the FT-IR spectrum of $NiMoO_4$ nano-powders. FT-IR spectrum containing a broad band between ~3500 and ~3700 cm^{-1} is due to the hydroxyl (O—H) stretching mode of water molecules adsorbed on the surface of the sample [23]. A band appears at 2350 cm^{-1} may be due to combination band of C—H or O—H stretching. Absorption band at 1513 cm^{-1} is due to the presence of O—H bending vibrations of adsorbed water molecule. The absorption band at 962 cm^{-1} can be assigned to symmetric stretching of Mo═O. The characteristic bands of $NiMoO_4$ appear at 485 and 650 cm^{-1} are assigned to Mo—O—Mo and Mo—O—Ni vibrations, respectively [23].

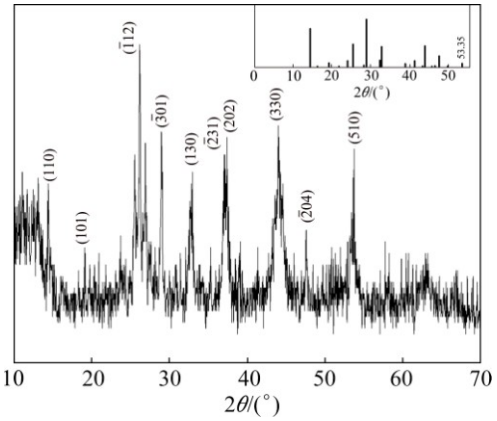

Fig. 1 XRD pattern of $NiMoO_4$ NPs

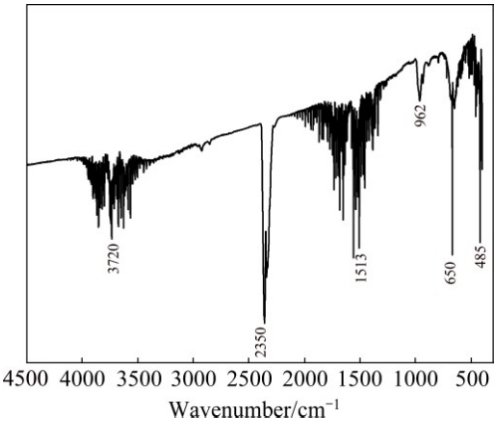

Fig. 2 FT-IR spectrum of $NiMoO_4$ NPs

3.3 SEM images

The surface morphology of $NiMoO_4$ sample was analyzed by SEM. Figures 3(a) and (b) show the SEM images of $NiMoO_4$ sample consisting of agglomerated particle-like nanostructure. The agglomeration of particles may be due to the attachment of magnetic nature of $NiMoO_4$. The elemental composition and purity of $NiMoO_4$ sample were also analyzed by energy dispersive X-ray method. Figure 3(c) shows the EDX spectrum of $NiMoO_4$ sample, which shows the presence of Ni, Mo and O by the appearance of Ni, Mo and O peaks without any other characteristic peaks. Hence, the EDX results are good evidence to draw a conclusion that the prepared $NiMoO_4$ does not contain any other elements and are certainly free from other impurities.

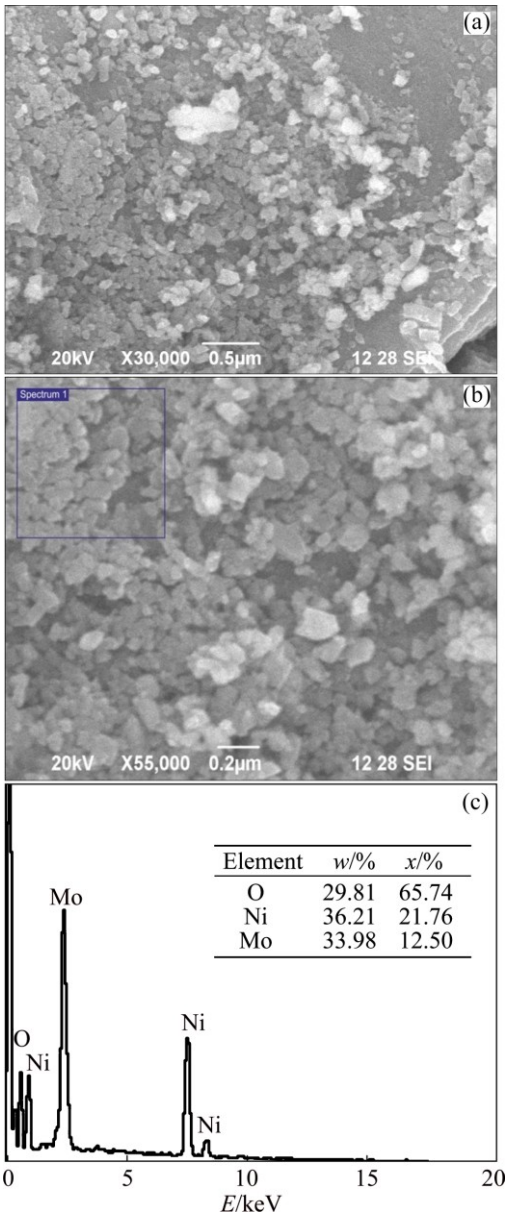

Fig. 3 SEM images (a, b) of $NiMoO_4$ NPs and EDX spectrum of $NiMoO_4$ NPs and elemental composition (c)

3.4 TEM images

Figure 4(a) depicts the TEM image of the as-prepared product, which indicates that the product belongs to nanosized particles. The particles size from TEM and SEM images was found to be in the range of 20−30 nm. The corresponding selected area electron diffraction (SAED) pattern (Fig. 4(b)) indicates the crystalline nature of the product.

3.5 Optical properties

UV−Vis absorption spectroscopy is an important technique for characterizing the optical properties of the prepared $NiMoO_4$ NPs. DRS analysis was used to study the relation between crystallite size and band gap of the semiconductors. UV−Vis DRS spectrum of $NiMoO_4$ nanoparticles is shown in Fig. 5. The steep shape of DRS

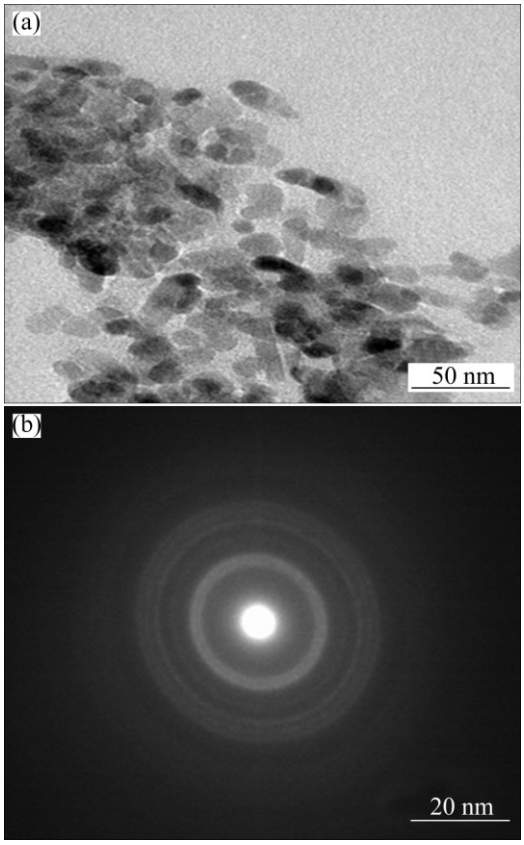

Fig. 4 TEM image (a) and selected area electron diffraction (SAED) pattern (b) of $NiMoO_4$ NPs

spectrum indicates that the visible-light absorption takes place from the band-gap transition instead of impurity levels [47,48]. The steep absorption edge was at 480 nm, corresponding to a band gap energy E_g of about 2.23 eV, indicating that the $NiMoO_4$ exhibited an intense absorption in the visible-light range. The band gap energy (E_g) of the sample can be evaluated using the Kubelka−Munk model. It permits the calculation of the absorption coefficient (α) by the measurement of the UV−Vis diffuse reflectance. Kubelka−Munk function, $F(R)$, is directly proportional to the absorption coefficient (α) and the value is estimated from the following equation [49]:

$$F(R)=\alpha=\frac{(1-R)^2}{2R} \tag{3}$$

where $F(R)$ is Kubelka−Munk function, α is the absorbance, and R is the the reflectance. A graph is plotted between $(F(R)h\upsilon)^2$ and $h\upsilon$, and the obtained intercept value is the band gap energy of the sample as shown in Fig. 5. The estimated band gap value of $NiMoO_4$ sample was found to be 2.23 eV. The E_g of 2.23 eV is much closer to 2.20 eV [23] of sample synthesized by conventional/microwave-assisted solvo-thermal method. Therefore, the observed different band

gaps by different preparation routes could not be resulted from the quantum-size effect, but can be attributed to their different degrees of crystallization [41]. The UV−Vis DRS spectra of $NiMoO_4$−TiO_2 nano-composite were also recorded and indicated that the band gap energy was 2.98 eV, which is higher than that of the pure $NiMoO_4$ (2.23 eV) and lower than that of pure TiO_2 (3.20 eV).

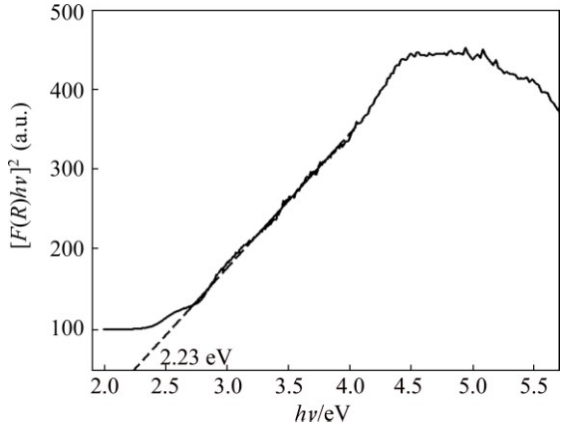

Fig. 5 UV−Vis diffuse reflectance spectra (DRS) of $NiMoO_4$ NPs

Photoluminescence (PL) emission is considered a powerful tool to obtain information on the electronic structure and degree of structural arrangements in medium range of the materials [50−53]. The PL spectrum of the $NiMoO_4$ nanostructures (Fig. 6) shows a broad band covering a large part of the visible spectrum with the maximum situated at 480 nm (blue emission). This PL profile suggests an emission mechanism characterized by the participation of several energy levels or light emission centers able to trap electrons within the band gap. However, the luminescence peaks were observed in the visible region at around 530, 545, and 565 nm, which are mainly due to the presence of radiative defects and oxygen vacancies of $NiMoO_4$ nanoparticles.

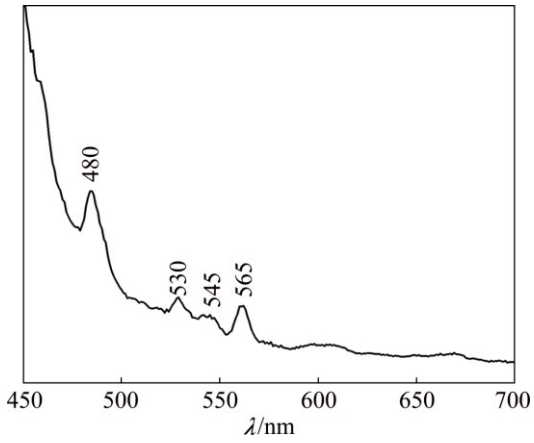

Fig. 6 Photoluminescence (PL) spectrum of $NiMoO_4$ NPs

3.6 Magnetic properties

Figure 7 shows the magnetic hysteresis (M−H) loop of $NiMoO_4$ nanoparticles with the field sweeping from −1200 to +1200 A/m at room temperature. The as-prepared $NiMoO_4$ nanoparticles show superparamagnetic behavior. $NiMoO_4$ nanoparticle is an important magnetic material. The saturation magnetization (M_s), remnant magnetization (M_r) and coercivity (H_c) values of the sample $NiMoO_4$ is 0.0187 $A{\cdot}m^2/kg$, 0.0052 $A{\cdot}m^2/kg$ and 2.3168×10^4 A/m, respectively. However, the magnetic properties of materials are influenced by many factors, such as size, crystallinity and surface structure.

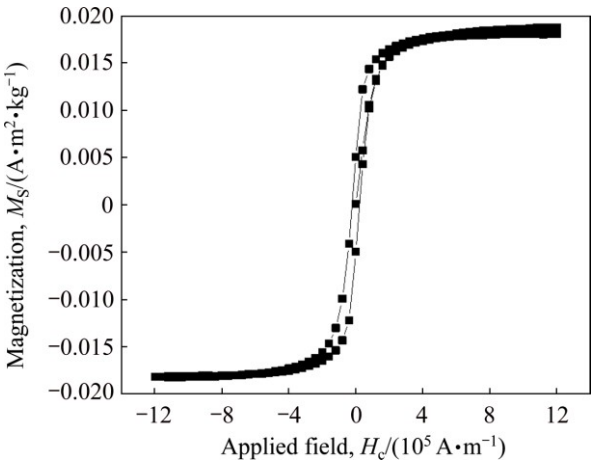

Fig. 7 Magnetic hysteresis (M−H) loop of $NiMoO_4$ NPs

3.7 Photocatalytic properties

The crystalline nature, size, shape and morphologies of the nano-materials are important factors that influence their photocatalytic activity. We prepared $NiMoO_4$ nano-photocatalysts to understand their catalytic activity of TiO_2-supported $NiMoO_4$−TiO_2 nanocompositie. In this study, we made an attempt to reveal the relationship between optical and photocatalytic properties of pure metal oxides ($NiMoO_4$ and TiO_2) and mixed metal oxides ($NiMoO_4$−TiO_2) and a series of experiments were carried out with 4-CP in aqueous suspension with light of wavelength 365 nm.

TiO_2-supported $NiMoO_4$ nano-photocatalyst on the PCD efficiency was evaluated, as shown in Fig. 8. The control experiment was carried out in the absence of catalyst by irradiating the solution with UV radiation (photolysis). The degradation of 4-CP due to photolysis was found to be less than 10%. The PCD efficiency of $NiMoO_4$ is lower compared with TiO_2. The PCD efficiency of TiO_2-supported $NiMoO_4$ (i.e., $NiMoO_4$−TiO_2) photocatalyst is higher than that of pure $NiMoO_4$ photocatalyst. It was found that the photocatalytic activity of single phase $NiMoO_4$ is enhanced when it is coupled with TiO_2 catalyst to form a composite catalyst [54,55]. Though the band gap of $NiMoO_4$ is smaller (2.23 eV) than that of TiO_2 (3.2 eV) and it is a

visible light active catalyst, it exhibits lower photocatalytic activity due to its lower valence band potential compared to TiO_2 [56]. The band gap of $NiMoO_4$−TiO_2 nanocomposite (2.98 eV) was found to be lower than that of pure TiO_2 (3.2 eV), exhibiting higher photocatalytic activity due to its lower valence band potential. When equimolar quantities of TiO_2 and $NiMoO_4$ are coupled and irradiated with UV−Vis light, the photocatalytic activity is improved though the charge carriers can migrate to $NiMoO_4$ due to the higher valence band potential of TiO_2. The degradation of 4-CP is believed to be initiated through the attacks by hydroxyl radicals at the phenyl group of 4-CP, which may result in the formation of intermediates that may be monohydroxylated or dihydroxylated 4-CP and followed by the cleavage of two-phenyl groups into intermediates. In addition, hydroquinone was the major intermediate.

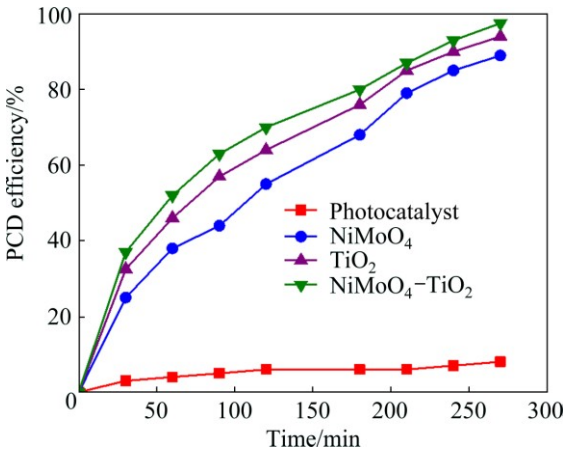

Fig. 8 Photocatalytic degradation (PCD) efficiency of TiO_2-supported $NiMoO_4$ photocatalyst (Experimental conditions: 50 mg/L 4-CP, 0.3 mg/mL photocatalyst, λ=365 nm, suspension pH 3)

The photo-degradation kinetics of 4-CP with and without $NiMoO_4$−TiO_2 nano-photocatalyst in the presence of UV light was evaluated using the pseudo first-order rate equation:

$$\ln(C_t/C_0) = -k_1 t \quad (4)$$

where C_0 is the initial concentration (mg/L), C_t is the concentration (mg/L) at time t, t is the UV light exposure time and k_1 is the first-order rate constant. The values of k_1 in relation to 4-CP concentration 50 and 1000 mg/L in the presence of $NiMoO_4$−TiO_2 catalyst were 1.87×10^{-2} and 0.94×10^{-2} min^{-1}, respectively, whereas the rate constants of the same reaction without catalyst were found to be 0.732×10^{-2} and 0.293×10^{-2} min^{-1}, respectively. The higher rate constant obtained using $NiMoO_4$−TiO_2 catalyst can be attributed to the combined effects of adsorption of 4-CP molecule over catalyst surface followed by oxidation using the generated hydroxyl radical and direct attack of photo-generated holes [57].

3.8 Reusability

The photocatalytic activity of $NiMoO_4$ was employed as a model reaction to investigate the reusability of $NiMoO_4$ and $NiMoO_4$−TiO_2 as nano-catalysts. The recycling of the catalyst is very important for industrial applications. The reusability of the catalysts for photo-degradation of 4-CP was evaluated and the results are shown in Fig. 9. For this purpose, the sample was filtered off from each run and washed several times with ethanol and dried at 70 °C in an air oven for 2 h and was checked for five consecutive runs under the same conditions, which indicates that these catalysts display good reproducibility and stability. From the results, it shows that the $NiMoO_4$ and $NiMoO_4$−TiO_2 nano-catalysts are highly active, highly recyclable, remarkably stable and environmentally friendly; they are promising candidates for the industrial and technological applications.

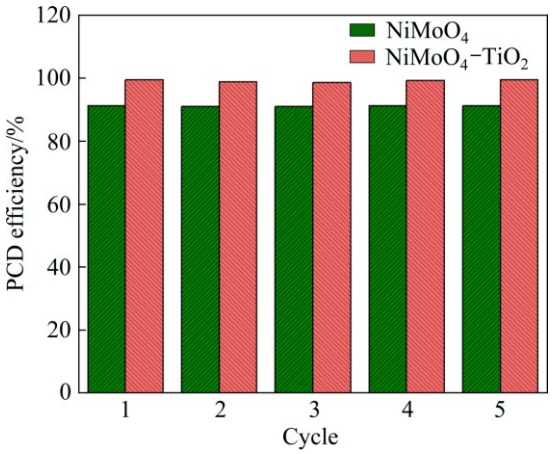

Fig. 9 Reusability of $NiMoO_4$ and $NiMoO_4$−TiO_2 nano-catalysts

4 Conclusions

1) $NiMoO_4$ nanoparticles were synthesized via sol−gel method using ethyl cellulose as surfactant. Powder XRD results indicated that pure single phase crystalline with monoclinic structure of $NiMoO_4$. The SEM and TEM images show that the morphology of the product consists of well-defined nanoparticles structure with agglomeration and the particle size in the range of 20−30 nm.

2) VSM results show superparamagnetic behavior. The PCD efficiency of TiO_2-supported $NiMoO_4$ (i.e., $NiMoO_4$−TiO_2) photocatalyst is higher than that of pure $NiMoO_4$ photocatalyst. These results indicate that $NiMoO_4$ nano-structures may find applications in water pollution control.

3) Compared to other synthetic methods, sol−gel method is a facile, low-cost pathway to synthesize novel $NiMoO_4$ nano-particles.

4) The monoclinic $NiMoO_4$ and $NiMoO_4$−TiO_2 nanophotacatalysts show photocatalytic efficiencies of 89.42 % and 97.68 % respectively for the degradation of 4-CP under the UV−Vis light irradiation.

Acknowledgements

The authors gratefully acknowledge the support from the Caplin Point Laboratories Limited, Chennai, India.

References

[1] ABDULLAH A, SALEEMI A S, ANIS-ur-REHMAN M. Comparative study of nano crystalline ceria synthesized by different wet-chemical methods [J]. Journal of Superconductivity and Novel Magnetism, 2014, 27: 273−276.

[2] KARAOGLU E, BAYKAL A. $CoFe_2O_4$–Pd(0) nanocomposite: Magnetically recyclable catalyst [J]. Journal of Superconductivity and Novel Magnetism, 2014, 27: 2041−2047.

[3] WANG Li-yan, WANG Hong-xia, WANG Ai-jie, LIU Min. Surface modification of a magnetic SiO_2 support and immobilization of a nano-TiO_2 photocatalyst on it [J]. Chinese Journal of Catalysis, 2009, 30: 939−944.

[4] KADDOURI A, ANOUCHINSKY R, MAZZOCCHIA C, MADEIRA L M, PORTELA M F. Oxidative dehydrogenation of ethane on the α and β phases of $NiMoO_4$ [J]. Catalysis Today, 1998, 40: 201−206.

[5] PILLAY B, MATHEBULA M R, FRIEDRICH H B. The oxidative dehydrogenation of *n*-hexane over Ni−Mo−O catalysts [J]. Applied Catalysis A, 2009, 361: 57−64.

[6] MADELEY R A, WANKE S E. Variation of the dispersion of active phases in commercial nickel−molybdenum/ γ-alumina hydrotreating catalysts during oxidative regeneration [J]. Applied Catalysis, 1988, 39: 295−314.

[7] GATES B C, KATZER J R, SCHUIT G C A. Chemistry of catalytic processes [M]. New York: McGraw-Hill, 1979: 390.

[8] PARK K S, SEO S D, SHIM H W, KIM D W. Electrochemical performance of $Ni_xCo_{1-x}MoO_4$ ($0\leq x\leq 1$) nanowire anodes for lithium-ion batteries [J]. Nanoscale Research Letters, 2012, 7: 35.

[9] XIAO Wei, CHEN Jun-song, LI Chang-ming, XU Rong, LOU Xiong-wen. Synthesis, characterization, and lithium storage capability of $AMoO_4$ (A=Ni, Co) nanorods [J]. Chemistry of Materials, 2010, 22: 746−754.

[10] SINGH R N, MADHU, AWASTHI R, SINHA A S K. Preparation and electrochemical characterization of a new $NiMoO_4$ catalyst for electrochemical O_2 evolution [J]. Journal of Solid State Electrochemistry, 2009, 13: 1613−1619.

[11] CHEN Ya-ping, LIU Bo-rui, LIU Qi, WANG Jun, LIU Jing-yuan, ZHANG Hong-sen, HU Song-xia, JING Xiao-yan. Flexible all-solid-state asymmetric supercapacitor assembled using coaxial $NiMoO_4$ nanowire arrays with chemically integrated conductive coating [J]. Electrochimica Acta, 2015, 178: 429−438.

[12] SAITO K, KAZAMA S, SATO Y, YUI T, YAGI M. Intercrystal self-assembly for the design of high-quality nickel molybdate nanocrystals [J]. Inorganic Chemistry, 2015, 54(18): 8869−8871.

[13] CAO Zhi, ZHANG Dao-jun, XU Chun-ying, ZHANG Ren-chun, YUAN Bai-qing. A novel enzyme-free glucose sensor based on nickel molybdate nanosheets [J]. International Journal of Electrochemical Science, 2015, 10(4): 3152−3159.

[14] CAI Dao-ping, WANG Dan-dan, LIU Bin, WANG Yan-rong, LIU Yuan, WANG Ling-ling, LI Han, HUANG Hui, LI Qiu-hong, WANG Tai-hong. Comparison of the electrochemical performance of $NiMoO_4$ nanorods and hierarchical nanospheres for supercapacitor applications [J]. Applied Materials & Interfaces, 2013, 5: 12905−12910.

[15] CHINNARAJ K, MANIKANDAN A, RAMU P, ARUL ANTONY S, NEERAJA P. Comparative studies of microwave and sol−gel-assisted combustion methods of Fe_3O_4 nanostructures: Structural, morphological, optical, magnetic, and catalytic properties [J]. Journal of Superconductivity and Novel Magnetism, 2015, 28: 179−190.

[16] AVILA JOSEPHINE B, MANIKANDAN A, MARY TERESITA V, ARUL ANTONY S. Fundamental study of $LaMg_xCr_{1-x}O_{3-\delta}$ perovskites nano-photocatalysts: Sol−gel synthesis, characterization and humidity sensing [J]. Korean Journal of Chemical Enggineering, 2016, 33: 1590−1598.

[17] MARY TERESITA V, MANIKANDAN A, AVILA JOSEPHINE B, SUJATHA S, ARUL ANTONY S. Electro-magnetic properties and humidity sensing studies of magnetically recoverable $LaMg_xFe_{1-x}O_{3-\delta}$ perovskites nano-photocatalysts by sol−gel route [J]. Journal of Superconductivity and Novel Magnetism, 2016, 29: 1691−1701.

[18] GHAED-AMINI M, BAZARGANIPOUR M, SALAVATI-NIASARI M, SABERYAN K. Morphology and photoluminescence of $BaMoO_4$ micro- and nano-crystals synthesized by coprecipitation method [J]. Transactions of Nonferrous Metals Society of China, 2015, 25: 3967−3973.

[19] KIANPOUR G, SOOFIVAND F, BADIEI M, SALAVATI-NIASARI M, HAMADANIAN M. Facile synthesis and characterization of nickel molybdate nanorods as an effective photocatalyst by co-precipitation method [J]. Journal of Materials Science: Materials in Electronics, 2016, 27: 10244−10251.

[20] ZHANG Dao-jun, ZHANG Ren-chun, XU Chun-ying, FAN Yong, YUAN Bai-qing. Microwave-assisted solvothermal synthesis of nickel molybdate nanosheets as a potential catalytic platform for NADH and ethanol sensing [J]. Sensors and Actuators B: Chemical, 2015, 206: 1−7.

[21] KLISSURSKI D, MANCHEVA M, IORDANOVA R, TYULIEV G, KUNEV B. Mechanochemical synthesis of nanocrystalline nickel molybdates [J]. Journal of Alloys and Compounds, 2006, 422: 53−57.

[22] ALBORZI A, KHADEMOLHOSEINI S. Nickel molybdate nanoparticles: Synthesis, characterization, optical and photocatalytic properties [J]. Journal of Materials Science: Materials in Electronics, 2016, 27: 3963−3967.

[23] de MOURA A P, de OLIVEIRA L H, ROSA I L V, XAVIER C S, LISBOA-FILHO P N, LI M S, la PORTA F A, LONGO E, VARELA J A. Structural, optical, and magnetic properties of $NiMoO_4$ nanorods prepared by microwave sintering [J]. The Scientific World Journal, 2015, 2015: 315084.

[24] SENTHILKUMAR B, SELVAN R K. Hydrothermal synthesis and electrochemical performances of 1.7 V $NiMoO_4{\cdot}xH_2O$||$FeMoO_4$ aqueous hybrid supercapacitor [J]. Journal of Colloid and Interface Science, 2014, 426: 280−286.

[25] AKIHIKO K, SATOSHI H. H_2 or O_2 evolution from aqueous solutions on layered oxide photocatalysts consisting of Bi^{3+} with $6s^2$ configuration and d^0 transition metal ions [J]. Chemistry Letters, 1999, 10: 1103−1104.

[26] FU Hong-bo, PAN Cheng-shi, YAO Wen-qing, ZHU Yong-fa. Visible-light-induced degradation of rhodamine B by nanosized Bi_2WO_6 [J]. Journal of Physical Chemistry B, 2005, 109: 22432−22439.

[27] ZHANG Shi-cheng, ZHANG Chuan, MAN Yi, ZHU Yong-fa. Visible-light-driven photocatalyst of Bi_2WO_6 nanoparticles prepared via amorphous complex precursor and photocatalytic properties [J]. Journal of Solid State Chemistry, 2006, 179: 62−69.

[28] ZHANG Shi-cheng, YAO Wen-qing, ZHU Yong-fa, SHI Li-yi. Preparation and photoelectrochemical properties of Bi_2WO_6 films with visible light response [J]. Acta Physico-Chimica Sinica, 2007, 23(1): 111−115.

[29] OLLIS D F, PELIZZETTI E, SERPONE N. Photocatalyzed destruction of water contaminants [J]. Environmental Science & Technology, 1991, 25: 1522−1529.

[30] HOFFMANN M R, MARTIN S T, CHOI W Y, BAHNEMANN D W. Environmental applications of semiconductor photocatalysis [J]. Chemical Reviews, 1995, 95: 69−96.

[31] HE Yu, ZHU Yong-fa, WU Nian-zu. Synthesis of nanosized $NaTaO_3$ in low temperature and its photocatalytic performance [J]. Journal of Solid State Chemistry, 2004, 177: 3868−3872.

[32] XU Tong-guang, ZHAO Xu, ZHU Yong-fa. Synthesis of hexagonal $BaTa_2O_6$ nanorods and influence of defects on the photocatalytic activity [J]. Journal of Physical Chemistry B, 2006, 110: 25825−25832.

[33] ZHANG Shi-cheng, ZHANG Chuan, YANG Hai-peng, ZHU Yong-fa. Formation and performances of porous $InVO_4$ films [J]. Journal of Solid State Chemistry, 2006, 179: 873−883.

[34] ZHANG Li-wu, FU Hong-bo, ZHANG Chuan, ZHU Yong-fa. Synthesis, characterization, and photocatalytic properties of $InVO_4$ nanoparticles [J]. Journal of Solid State Chemistry, 2006, 179: 804−811.

[35] UMAPATHY V, MANIKANDAN A, ARUL ANTONY S, RAMU P, NEERAJA P. Structure, morphology and opto-magnetic properties of Bi_2MoO_6 nano-photocatalyst synthesized by sol−gel method [J]. Transactions of Nonferrous Metals Society of China, 2015, 25: 3271−3278.

[36] UMAPATHY V, MANIKANDAN A, ARUL ANTONY S, RAMU P, NEERAJA P. Synthesis and characterization of $Fe_2(MoO_4)_3$ nano-photocatalyst by simple sol−gel method [J]. Journal of Nanoscience and Nanotechnology, 2016, 16: 987−993.

[37] UMAPATHY V, NEERAJA P: Sol−gel synthesis and characterizations of $CoMoO_4$ nanoparticles: An efficient photocatalytic degradation of 4-chlorophenol [J]. Journal of Nanoscience and Nanotechnology, 2016, 16: 2960−2966.

[38] FU Hong-bo, ZHANG Li-wu, YAO Wen-qing, ZHU Yong-fa. Photocatalytic properties of nanosized Bi_2WO_6 catalysts synthesized via a hydrothermal process [J]. Applied Catalysis B, 2006, 66: 100−110.

[39] ZHAO Xu, XU Tong-guang, YAO Wen-qing, ZHANG Chuan, ZHU Yong-fa. Photoelectrocatalytic degradation of 4-chlorophenol at Bi_2WO_6 nanoflake film electrode under visible light irradiation [J]. Applied Catalysis B, 2007, 72: 92−97.

[40] HUANG Guang-li, ZHANG Chuan, ZHU Yong-fa. $ZnWO_4$ photocatalyst with high activity for degradation of organic contaminants [J]. Journal of Alloys and Compounds, 2007, 432: 269−276.

[41] ZHAO Xu, YAO Wen-qing, WU Yan, ZHANG Shi-cheng, YANG Hai-peng, ZHU Yong-fa. Fabrication and photoelectrochemical properties of porous $ZnWO_4$ film [J]. Journal of Solid State Chemistry, 2006, 179: 2562−2570.

[42] TADJARODI A, PRADEHKHORRAM R, IMANI M, EBRAHIMI S, SALEHI M. A simplified microwave-assisted synthesis of $NiMoO_4$ nanoparticles by using organic driving agent and study of photocatalytic activity [C]//Proceedings of the 18th International Electronic Conference on Synthetic Organic Chemistry (ECSOC-18). Basel: MDPI, 2014.

[43] DING Yi, WAN Yong, MIN Yu-lin, ZHANG Wei, YU Shu-hong. General synthesis and phase control of metal molybdate hydrates $MMoO_4{\cdot}nH_2O$ (M=Co, Ni, Mn, n=0, 3/4, 1) nano/microcrystals by a hydrothermal approach: Magnetic, photocatalytic, and electrochemical properties [J]. Inorganic Chemistry, 2008, 47(17): 7813−7823.

[44] HAETGE J, DJERDJ I, BREZESINSKI T. Nanocrystalline $NiMoO_4$ with an ordered mesoporousmorphology as potential material for rechargeable thin film lithium batteries [J]. Chemical Communications, 2012, 48(53): 6726−6728.

[45] ZĂVOIANU R, DIAS C R, PAULA A, SOARES V, PORTELA M F. Oxidative dehydrogenation of i-butane over nanostructured silica-supported NiMoO4 catalysts with low content of active phase [J]. Applied Catalysis A, 2006, 298: 40−49.

[46] MAZZOCCHIA C, ABOUMRAD C, DIAGNE C, TEMPESTI E, HERRMANN J M, THOMAS G. On the $NiMoO_4$ oxidative dehydrogenation of propane to propene: Some physical correlations with the catalytic activity [J]. Catalysis Letters, 1991, 10(3−4): 181−191.

[47] YOSHIKI S, HIDEKI K, HISAYOSHI K, AKIHIKO K. Photophysical properties and photocatalytic activities of bismuth molybdates under visible light irradiation [J]. Journal of Physical Chemistry B, 2006, 110: 17790−17797.

[48] KUDO A, TSUJI I, KATO H. $AgInZn_7S_9$ solid solution photocatalyst for H_2 evolution from aqueous solutions under visible light irradiation [J]. Chemical Communications, 2002, 17: 1958−1959.

[49] MANIKANDAN A, SRIDHAR R, ARUL ANTONY A, RAMAKRISHNA S. A simple aloe vera plant-extracted microwave and conventional combustion synthesis: Morphological, optical, magnetic and catalytic properties of $CoFe_2O_4$ nanostructures [J]. Journal of Molecular Structure, 2014, 1076: 188−200.

[50] NOGUEIRA I C, CAVALCANTE L S, PEREIRA P F S, de JESUS M M, RIVAS MERCURY J M, BATISTA N C, LI M S, LONGO E. Rietveld refinement, morphology and optical properties of $(Ba_{1-x}Sr_x)MoO_4$ crystals [J]. Journal of Applied Crystallography, 2013, 46(5): 1434−1446.

[51] SCZANCOSKI J C, BOMIO M D R, CAVALCANTE L S, JOYA M R, PIZANI P S, J. VARELA J A, LONGO E, SIU LI M, ANDRÉS J A. Morphology and blue photoluminescence emission of $PbMoO_4$ processed in conventional hydrothermal [J]. Journal of Physical Chemistry C, 2009, 113(14): 5812−5822.

[52] MARQUES V S, CAVALCANTE L S, SCZANCOSKI J C, ALCÂNTARA A F P, ORLANDI M O, MORAES E, LONGO E, VARELA J A, SIU LI M, SANTOS M R M C. Effect of different solvent ratios (water/ethylene glycol) on the growth process of $CaMoO_4$ crystals and their optical properties [J]. Crystal Growth & Design, 2010, 10(11): 4752−4768.

[53] LONGO V M, CAVALCANTE L S, PARIS E C, SCZANCOSKI J C, PIZANI P S, LI M S, ANDRÉS J, LONGO E, VARELA J A. Hierarchical assembly of $CaMoO_4$ nano-octahedrons and their photoluminescence properties [J]. Journal of Physical Chemistry C, 2011, 115(13): 5207−5219.

[54] XU Shi-hong, FENG Dao-lun, SHANGGUAN Wen-feng. Preparations and photocatalytic properties of visible-light-active zinc ferrite-doped TiO_2 photocatalyst [J]. Journal of Physical Chemistry C, 2009, 113: 2463−2467.

[55] MOHAMED R M, AAZAM E. Synthesis and characterization of P-doped TiO_2 thin-films for photocatalytic degradation of butyl benzyl phthalate under visible-light irradiation [J]. Chinese Journal of Catalysis, 2013, 34: 1267−1273.

[56] HANKARE P P, PATIL R P, JADHAV A V, GARADKAR K M, SASIKALA R. Enhanced photocatalytic degradation of methyl red and thymol blue using titania−alumina−zinc ferrite nanocomposite

[J]. Applied Catalysis B, 2011, 107: 333−339.
[57] AHMED S, RASUL M G, MARTENS W N, BROWN R, HASHIB M A. Heterogeneous photocatalytic degradation of phenols in wastewater: A review on current status and developments [J]. Desalination, 2010, 261: 3−18.

$NiMoO_4$纳米颗粒的溶胶−凝胶法合成及其组织、形貌、光学、磁学和光催化性能

V. UMAPATHY[1,2], P. NEERAJA[3], A. MANIKANDAN[4], P. RAMU[5]

1. Research and Development Centre, Bharathiar University, Coimbatore, Tamil Nadu 641046, India;
2. Caplin Point Laboratories Limited, Chennai 600017, India;
3. Department of Chemistry, NKR Government Arts College for Women, Namakkal, Tamil Nadu 637001, India;
4. Department of Chemistry, Bharath Institute of Higher Education and Research, Bharath University, Chennai 600073, India;
5. Department of Chemistry, Meenakshi Academy of Higher Education and Research, Chennai, Tamil Nadu 600078, India

摘　要：采用溶胶−凝胶法合成钼酸镍($NiMoO_4$)纳米颗粒。以水作为溶剂使所得产品具有纳米晶结构。使用 X 射线衍射、能量分散 X 射线分析(EDX)和傅里叶转换红外光谱等手段对纳米晶进行结构表征。使用扫描电镜和透射电镜对纳米晶颗粒的尺寸大小和形貌进行观察。结果表明，所得纳米颗粒和纯度较高，为单相单斜结构。采用紫外−可见漫反射光谱(UV−Vis−DRS)和光致发光测量法研究室温下产品的光学性能。采用振动样品磁强计(VSM)研究样品的磁性能。结果显示，所得样品具有超顺磁行为。考察了 $NiMnO_4$ 样品的光催化活性。结果显示，添加 TiO_2 能提高 $NiMnO_4$ 的光催化活性。测定了催化剂 $NiMnO_4$、TiO_2 和 $NiMoO_4$−TiO_2 纳米颗粒对 4-氯酚(4-CP)的光催化降解行为。光催化降解结果显示，$NiMoO_4$−TiO_2 纳米颗粒的光催化降解效率高于 $NiMnO_4$ 和 TiO_2 的。

关键词：$NiMnO_4$；TiO_2；纳米结构；溶胶−凝胶合成；光学性能；磁学性能；光催化；单斜结构

(Edited by Wei-ping CHEN)